2^{nd} *Int. Symposium on Turbulence Heat and Mass Transfer, pp. 481-490*
K. Hanjalić, T.W.J. Peeters (Editors)

LES of Recirculating Flow Without Any Homogeneous Direction: A Dynamic One-Equation Subgrid Model

Lars Davidson
Thermo and Fluid Dynamics, Chalmers University of Technology
S-412 96 Gothenburg, Sweden

Abstract — Standard dynamic subgrid models have numerical stability problems. The remedy is to average in some homogeneous flow direction(s) or to introduce some artificial clipping. Thus this type of models do not seem to be applicable to real three-dimensional flow without introducing *ad hoc* user modifications. In the present study a first attempt to formulate a new one-equation subgrid model is presented which reduces the need of this type of user-modifications. The model is applied to recirculating flow in an enclosure.

1. Introduction

Germano *et al.* [1, 2] propose a dynamic subgrid model in which the constant in the Smagorinsky model is not arbitrarily chosen (or optimized), but where it is computed. The dynamic models which have been developed have problems with negative values of the C-coefficient. When a negative C occurs it is believed to represent *backscatter*, i.e. spectral flow of energy from subgrid scales to resolved scales. This means that the production term in the transport equation for subgrid kinetic energy $P_{k_{sgs}} = -\tau_{ij}^a \bar{u}_{i,j}$ becomes negative, and feeds energy back to the resolved scales. The problem is that negative diffusion (negative C) causes numerical problems. These can be handled as long as the total (i.e. viscous plus turbulent) diffusion is positive. However, large negative, turbulent diffusion remains a problem. It is not only negative values on C that causes numerical problems. It exhibits very strong gradient and "fluctuates wildly" [3]. In a ventilated enclosure, for example, the author has found that C varies typically in the range ± 4 which should be compared with a standard value of the Smagorinsky constant $C_S^2 = 0.01$. In the literature [3, 4, 5, 6, 7, 8, 9, 10, 11] it has been found that in order to achieve numerical stability present dynamic subgrid models require either that there exist a homogeneous flow direction or that the dynamic coefficient is clipped at some arbitrary limit in an *ad hoc* manner. Thus the model does not seem to be applicable to real three-dimensional flows where no homogeneous flow direction exists.

An attempt to improve this restriction was presented by Ghosal *et al.* [12, 13] where they try to optimize the equation for C globally, but still with the constraint that $C > 0$. This optimization leads to an integral equation (Fredholm's integral equation of the second kind) which is very expensive to solve numerically. They report that it increases the CPU time by 50% [14].

In the present work a new one-equation dynamic subgrid model is applied to recirculating flow in an enclosure.

2. The Dynamic One-Equation Subgrid Model

If we follow Germano [16] and introduce *generalized* central moments the transport equation for the subgrid kinetic energy k_{sgs} reads [15]

$$\frac{\partial k_{sgs}}{\partial t} + (\bar{u}_j k_{sgs})_{,j} = -\mathcal{T}_f(u_i,u_j)\bar{u}_{i,j} - \left\{\frac{1}{2}\mathcal{T}_f(u_j,u_i,u_i) + \mathcal{T}_f(u_j,p)\right\}_{,j} + \nu(k_{sgs})_{,jj} - \nu\mathcal{T}_f(u_{i,j},u_{i,j}). \tag{1}$$

The dynamic coeffi cient C in the production term

$$P_{k_{sgs}} = -\tau^a_{ij}\bar{u}_{i,j},\ \tau^a_{ij} \equiv \mathcal{T}_f(u_i,u_j) = -2C\Delta k^{\frac{1}{2}}_{sgs}\bar{S}_{ij} \tag{2}$$

is computed in a similar way as in the standard dynamic model [1, 2, 12, 13], i.e.

$$\begin{aligned} C &= -\frac{\mathcal{L}_{ij}M_{ij}}{2M_{ij}M_{ij}};\ \mathcal{L}_{ij} = \widehat{\bar{u}_i\bar{u}_j} - \widehat{\bar{u}}_i\widehat{\bar{u}}_j;\ K = k_{sgs} + \frac{1}{2}\mathcal{L}_{ii} \\ M_{ij} &= \widehat{\Delta}\widehat{K^{\frac{1}{2}}}\widehat{\bar{S}}_{ij} - \Delta\widehat{k^{\frac{1}{2}}_{sgs}\bar{S}_{ij}} \end{aligned} \tag{3}$$

where $\mathcal{L}_{ij}$ denotes the *dynamic* Leonard stresses, and where $K \equiv \frac{1}{2}T_{ii}$ is the subgrid kinetic energy on the test level [12, 13, 15]. The diffusion constant can also be computed dynamically as in Refs. [12, 13]. In the present study the standard gradient hypothesis is used with the turbulent Prandtl number set to one. The dissipation term $\varepsilon_{k_{sgs}}$ is estimated as

$$\varepsilon_{k_{sgs}} \equiv \nu\mathcal{T}_f(u_{i,j},u_{i,j}) = C_*\frac{k^{\frac{3}{2}}_{sgs}}{\Delta}. \tag{4}$$

In order to estimate C_* attention is turned to the transport equation for K. The equations for k_{sgs} and K read in symbolic form

$$C_{k_{sgs}} - D_{k_{sgs}} = P_{k_{sgs}} - C_*\frac{k^{\frac{3}{2}}_{sgs}}{\Delta},\ \ C_K - D_K = P_K - C_*\frac{K^{\frac{3}{2}}}{\widehat{\Delta}} \tag{5a, b}$$

Apply the test fi lter to Eq. 5a. If we, similar to what is done in the Algebraic Reynolds Stress model (ASM) [17, 18], assume that the transport of k_{sgs} is proportional to that of K with the constant of proportionality $\widehat{k}_{sgs}/K$, Eq. 5 give

$$\widehat{P}_{k_{sgs}} - \frac{1}{\Delta}\widehat{C_*k^{\frac{3}{2}}_{sgs}} = \frac{\widehat{k}_{sgs}}{K}\left(P_K - C_*\frac{K^{\frac{3}{2}}}{\widehat{\Delta}}\right), \tag{6}$$

and we obtain

$$C^{n+1}_* = \left(P_K - \widehat{P}_{k_{sgs}} + \frac{1}{\Delta}\widehat{C^n_*k^{\frac{3}{2}}_{sgs}}\right)\frac{\widehat{\Delta}}{K^{\frac{1}{2}}\widehat{k}_{sgs}} \tag{7}$$

The dissipation cannot be negative which requires that we limit C_* to positive values, i.e. $C_* \geq 0$. In Eq. 7 C_* is kept inside the fi ltering process. Following Piomelli [6] the dynamic coeffi cient under the fi lter is taken at the old time-step.

To ensure numerical stability a *constant* value of C in space ($\langle C \rangle_{xyz}$) is used in the momentum equations, which is determined by requiring that the production in the whole computational domain should remain the same, i.e.

$$\langle 2C\Delta k_{sgs}^{\frac{1}{2}} \bar{S}_{ij} \bar{S}_{ij} \rangle_{xyz} = 2\langle C \rangle_{xyz} \langle \Delta k_{sgs}^{\frac{1}{2}} \bar{S}_{ij} \bar{S}_{ij} \rangle_{xyz} \tag{8}$$

The idea is to include all local dynamic information through the source terms of the transport equation for k_{sgs}. This is probably physically more sound since large local variations of C appear only in the source term, and the effect of the large fluctuations in the dynamic coefficients will be smoothed out in a natural way. This means that the need to restrict or limit the dynamic coefficient is reduced or may not be necessary altogether. However, *if* we have to restrict the dynamic coefficients in the k_{sgs} equation this does not affect the results as much as if the coefficient in the original dynamic model is restricted. The reason is that in the one-equation model the coefficients affect the stresses only in an indirect way (the source terms are part of a transport equation) whereas in the original dynamic model the dynamic coefficient is linearly proportional to the stresses. It is extremely important to use subgrid models which are numerically stable and where the need to introduce *ad hoc* modification is limited as far as possible, if we want to develop turbulence models applicable to general flow situations.

The spatial variation of C is included via the production term in the modelled k_{sgs} equation. In this way backscatter is taken into account in an indirect way. Although it is not fed *directly* back to the resolved flow, it influences the resolved flow via the kinetic subgrid energy. A negative production reduces k_{sgs} and this effect influences the neighborhood through convection and diffusion of k_{sgs}.

The new model can be summarized as follows:

1. The equation for the kinetic subgrid energy is solved (Eq. 1);

2. The production term (see Eq. 2) is computed using the *local* dynamic coefficient (Eq. 3) without any averaging or restrictions;

3. The turbulent Prandtl number in the diffusion term is set to one;

4. The local dynamic coefficient in front of the dissipation term is computed from Eq. 7;

5. The subgrid stresses in the momentum equation are computed using a *homogeneous* values $\langle C \rangle_{xyz}$ of the dynamic coefficient determined from Eq. 8; $\langle C \rangle_{xyz}$ is also used in the diffusion term in the k_{sgs} equation.

6. The boundary condition for k_{sgs} is zero at all boundaries.

The boundary conditions for k_{sgs} does not seem to affect the results much, and the reason is that the equation is dominated by its source terms, production and dissipation (see Fig. 7b).

Some limits on C_* *are used*. It is not allowed to go negative (this occurs in approximately 10% of the nodes). A limit is also used to prevent C_* from growing too large. Presently an arbitrary value of 10 is used; this limit is reached in approximately 25% of the nodes (see Eq. 4b), which is much too much.

3. The Numerical Method

An implicit, two-step time-advancement methods is used. When the filtered Navier-Stokes equation for $\bar{u}_i$

$$\frac{\partial \bar{u}_i}{\partial t} + \frac{\partial}{\partial x_j}(\bar{u}_i \bar{u}_j) = -\frac{1}{\rho}\frac{\partial \bar{p}}{\partial x_i} + \nu \frac{\partial^2 \bar{u}_i}{\partial x_j \partial x_j} - \frac{\partial \tau_{ij}}{\partial x_j} \tag{9}$$

is discretized it can be written

$$\bar{u}_i^{n+1} = \bar{u}_i^n + \Delta t H\left(u_i^n, u_i^{n+1}\right) - \frac{1}{\rho}\alpha\Delta t\frac{\partial p^{n+1}}{\partial x_i} - \frac{1}{\rho}(1-\alpha)\Delta t\frac{\partial p^n}{\partial x_i} \tag{10}$$

where $H\left(u_i^n, u^{n+1}\right)$ includes convection and the viscous and subgrid stresses, and $\alpha = 0.5$ (Crank-Nicolson). Equation 10 is solved which gives $\bar{u}_i^{n+1}$ which does not satisfy continuity. An intermediate velocity field is computed by subtracting the implicit part of the pressure gradient, i.e.

$$\bar{u}_i^* = \bar{u}_i^{n+1} + \frac{1}{\rho}\alpha\Delta t\frac{\partial p^{n+1}}{\partial x_i}. \tag{11}$$

Taking the divergence of Eq. 11 requiring that continuity (for the face velocities which are obtained by linear interpolation) should be satisfied on level $n+1$, i.e. $\partial\bar{u}_{i,f}^{n+1}/\partial x_i = 0$ we obtain

$$\frac{\partial^2 p^{n+1}}{\partial x_i \partial x_i} = \frac{\rho}{\Delta t\alpha}\frac{\partial \bar{u}_{i,f}^*}{\partial x_i}. \tag{12}$$

The numerical procedure at each time step can be summarized as follows [19].

1. Solve the discretized filtered Navier-Stokes equation for $\bar{u}$, $\bar{v}$ and $\bar{w}$.

2. Create an intermediate velocity field $\bar{u}_i^*$ from Eq. 11.

3. The Poisson equation (Eq. 12) is solved with an efficient multigrid method [20].

4. Compute the face velocities (which satisfy continuity) from the pressure and the intermediate velocity as

$$\bar{u}_{i,f}^{n+1} = \bar{u}_{i,f}^* - \frac{1}{\rho}\alpha\Delta t\left(\frac{\partial p^{n+1}}{\partial x_i}\right)_f. \tag{13}$$

5. Step 1 to 4 is performed till convergence (normally two or three iterations) is reached.

6. The turbulent viscosity is computed.

7. Next time step.

Please note that although no explicit dissipation is added to prevent odd-even decoupling, an implicit dissipation is present. The intermediate velocity field is computed at the *nodes* (see Eq. 11) subtracting a pressure gradient. When, after having solved the pressure Poisson equation, the face velocity field is computed a pressure gradient at the *faces* (see Eq. 13) is added. This is very similar to the Rhie-Chow dissipation [21].

4. Results

A steady computation is first carried out using the CALC-BFC code and the $k-\varepsilon$ model [22]. These results are used as initial start fields in the LES calculations. The predictions are compared with Laser-Doppler measurements of Restivo [23] (also available in Ref. [24]). The geometry is given by (see Fig. 1:

$$L/H = 3,\ W/H = 1,\ h/H = 0.056,\ t/H = 0.16,\ Re = \frac{U_{in}h}{\nu} = 5000$$

We have used $H = 3$ m, $U_{in} = 0.455$ m/s, and air of 20^{o}C. Inlet boundary conditions are set as

$$\bar{u}_{in} = U_{in} + random \cdot u_{rms,exp},\ \bar{v}_{in} = random \cdot u_{rms,exp},\ \bar{w}_{in} = random \cdot u_{rms,exp} \tag{14}$$

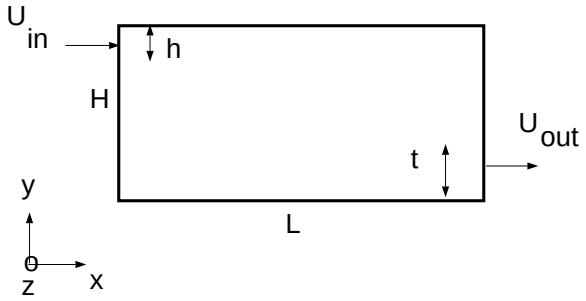

Figure 1: Ventilated enclosure.

$\Delta x_{min}/H$	$\Delta y_{min,f}/H$	$\Delta y_{min,c}/H$	$\Delta z_{min}/H$	$\Delta x_{max}/H$	$\Delta y_{max}/H$	$\Delta z_{max}/H$
0.0084	0.015	0.0013	0.0074	0.061	0.033	0.025

Table 1: Geometrical details of the mesh. The min distances denote the extent of the control volume near the wall. Index c and f denote ceiling and fbor, respectively.

Note that the random function is called at different times for $\bar{u}_{in}$, $\bar{v}_{in}$ and $\bar{w}_{in}$, which means that the fluctuations are not correlated so that $(\overline{\bar{u}\bar{v}})_{in} = (\overline{\bar{u}\bar{w}})_{in} = (\overline{\bar{v}\bar{w}})_{in} = 0$.

At the outlet the exit velocity is computed from global continuity and it is taken as constant over the outlet. Zero gradient is set for the remaining variables.

At all six walls traditional wall functions [22] are used if $y^+ > 11$. Along the ceiling these are never used as the boundary layer is well resolved ($y^+ < 3$ for the first node).

A $96 \times 64 \times 64$ grid has been used. A hyperbolic tangent function is used in x and z direction, whereas geometric stretching is used in the y direction. At the position $x/H = 2$ (see Fig. 5) 17 nodes are located inside the velocity maximum, $y_{1/2}$ corresponds to $y/H = 0.89$, and for the near-wall node $y^+ \simeq 2$. For more details, see Table 1. Results using other meshes are presented in Refs. [9, 22]. The number of time steps used in each calculation is typically 40000 using a maximum CFL number of two. This corresponds to approximately 2200 seconds. The streamwise average of the peak velocity in the wall jet along the ceiling is close to $U_{av} = 0.5U_{in}$ ($= 0.228$ m/s). Thus the time it takes for a fluid particle to move from the inlet to the opposite wall can be estimated as $L/U_{av} \simeq 40$ seconds, which means that $2200/40 = 55$ characteristic time units (L/U_{av}) are covered in a simulation. All results presented below have been obtained using 40 000 time steps. Averaging has been performed during the last 15 000 or 20 000 time steps. Tests presented in [22] show that this is more than enough. Unless otherwise stated all results presented have been obtained with the new dynamic one-equation model.

In Fig. 2 the time averaged $\bar{u}$ velocities and resolved fluctuations are compared with experiments, and as can seen the agreement is reasonably good. The predicted peak velocity in the wall jet is slightly too low and the width of the wall jet is somewhat over-predicted. The original dynamic model [1, 2, 22] is compared with the new dynamic one-equation model and the predicted results are comparable.

The time history of $\bar{u}$ and k_{sgs} are shown in Fig. 3. From the time history of $\bar{u}$ there seems to be some large structures present with a cycle of 200 to 250 seconds. The subgrid turbulent kinetic energy k_{sgs} is generally small with some peaks.

From the time history of the homogeneous dynamic coefficient $\langle C \rangle_{xyz}$ in Fig. 4a we find that the time averaged value is close to 0.05 which corresponds to a value of the Smagorinsky

constant $C_S = 0.22$. The coefficient rather often wants to go negative, but it is clipped at zero. The C_* coefficient connected with the dissipation term in the k_{sgs} equation is presented in Fig. 4b. It is shown during a short time in order to visualize its behavior. It can be seen that it very often hits its limits zero and 10, which is not desirable. Looking at its equation (Eq. 7) we find that there is a strong positive feedback between k_{sgs} and the C_* coefficient. If k_{sgs} goes towards zero, the coefficient C_* increases sharply and thereby increases the dissipation term in the k_{sgs} equation (Eq. 1), which decreases k_{sgs} even more. Vice versa if k_{sgs} increases: the coefficient C_* decreases and as a result the dissipation term decreases and k_{sgs} increases even more. This is what we see in Fig. 4b. When C_* starts to decrease the positive feedback enhances this tendency and C_* hits the lower limit; vice versa if the coefficient increases. Thus the form used in Eq. 7 does not seem to be very suitable.

4.1. Wall jet

The flow along the ceiling is a wall jet. Thus it could be interesting to compare with wall jet data. The experiments of Karlsson *et al.* [25] have been chosen. The Reynolds number in the wall jet experiment is higher ($Re = 10000$) than in the present study.

In Fig. 5 the streamwise mean velocities, computed with the standard dynamic model and the one-equation dynamic model, are compared with experiments, and the agreement is very good. If we, however, compare the width and the maximum velocities this picture changes. The predicted wall jet spreads too much and the peak velocity is predicted too low compared with experiments (see Table 2), which agrees with the comparison in Fig. 2. The reason for the rather poor agreement could be due to insufficient grid. It could also be that the subgrid models (both the dynamic and the dynamic one-equation model) give too low a subgrid viscosity. As a results this would give too large exchange of momentum in the y direction due to too little damping (by the subgrid stresses) of the resolved fluctuations.

The stresses in the wall jet are shown in Fig. 6. The predicted streamwise stress agrees well with experiments in the outer region. The minimum (in the region of the maximum velocity) is not well captured. The predicted $\langle v''v'' \rangle_t$ is too low compared to experiments. The predicted shear stress is in good agreement with the experimental one. The stress changes sign near the wall and the location agrees well with the experimental one; the positive peak, however, is under-predicted. The dynamic Leonard stress $\mathcal{L}_{12}$ (see Eq. 3) is also included. It is interesting to note that in the region where the velocity attains it maximum and the resolved shear stress

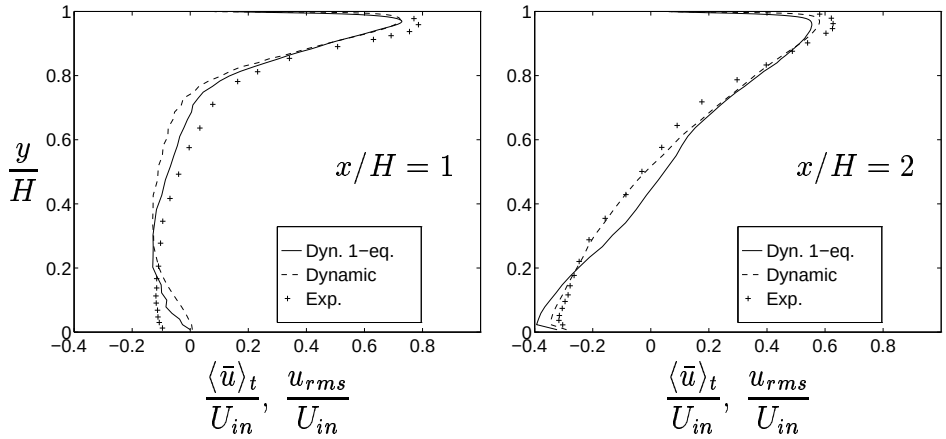

Figure 2: Time averaged velocity and resolved rms profiles. Symmetry plane $z/H = 0.5$. Solid lines: $\langle \bar{u} \rangle_t / U_{in}$; dashed lines: u_{rms}/U_{in}; $+$: experimental mean velocity; $\circ$: experimental rms.

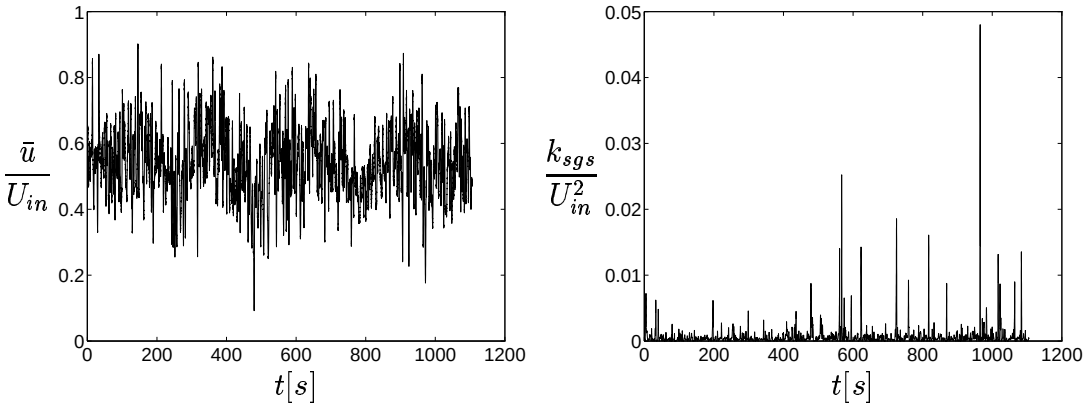

Figure 3: Time history of $\bar{u}$ and k_{sgs} at one chosen cell. $x/H = 2.0, y/H = 0.92$, $z/H = 0.5$.

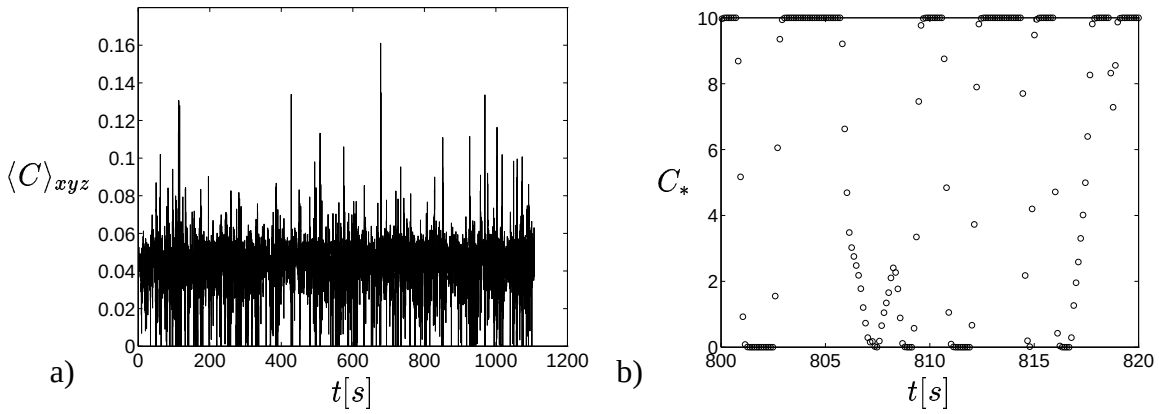

Figure 4: Time history of the dynamic coeffi cients. a) The dynamic coeffi cient $\langle C \rangle_{xyz}$. b) The dynamic coeffi cient C_* at one chosen cell $x/H = 2.0, y/H = 0.92, z/H = 0.5$.

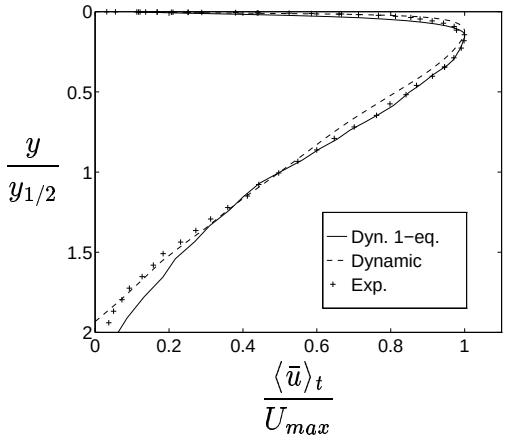

Figure 5: Time averaged velocity. $z/H = 0.5$. LES: $x/H = 2$ ($x/h = 35.7$); exp: $x/h = 40$. Solid line: 1-eq. dynamic model; dashed line: dynamic model; $+$: experiments [25].

	x/h	U_{max}/U_{in}	$d\delta_{1/2}/dx$	$y_{1/2}/h$	$y(U_{max})/h$
LES	17.9	0.718	-	2.23	0.51
LES	35.7	0.545	0.12	4.51	0.64
Exp.	20	0.771	-	1.88	0.35
Exp.	40	0.566	0.08	3.48	0.55

Table 2: Comparison with wall jet data [25]

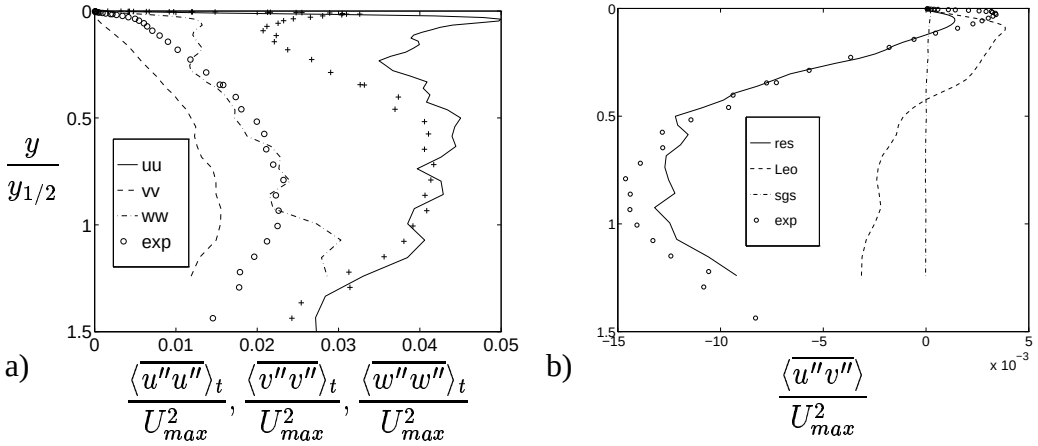

Figure 6: Resolved stresses. Symmetry plane $z/H = 0.5$. LES: $x/H = 2$ ($x/h = 35.7$); exp: $x/h = 40$. a) Solid line: $\langle u''u''\rangle_t/U_{max}^2$; dashed line: $\langle v''v''\rangle_t/U_{max}^2$; dash-dotted line: $\langle w''w''\rangle_t/U_{max}^2$. $+$: experimental $\overline{u^2}/U_{max}^2$; $\circ$: experimental $\overline{v^2}/U_{max}^2$ [25]. b) Solid line: shear stress $\langle u''v''\rangle_t/U_{in}^2$; dashed line: dynamic Leonard stress $\langle\mathcal{L}_{12}\rangle_t/U_{in}^2$; dash-dotted line: subgrid shear stress $\langle\tau_{12}\rangle_t/U_{in}^2$; $\circ$: experimental $\overline{uv}/U_{max}^2$[25].

changes sign, $\mathcal{L}_{12}$ is considerably larger than the resolved stress (this is also seen for the turbulent kinetic energies in Fig. 7a). It can be seen that the subgrid stress is much smaller than the resolved stress. Actually, at $x/h = 40$, the time averaged subgrid turbulent viscosity is of the same order as the viscous one ($\langle\nu_{sgs}\rangle < 2\nu$), whereas the instantaneous value can be much higher ($\nu_{sgs,max} \simeq 23\nu$).

In Fig. 7a turbulent kinetic energies are presented. We find that the subgrid energy k_{sgs} is much smaller than the resolved one, but it is not negligible. The dynamic Leonard kinetic energy is a large fraction of the resolved kinetic energy and, as was the case for the shear stress in Fig. 6b, it exceeds the resolved kinetic energy near the region of the velocity maximum. In Fig. 7b the time averaged production and dissipation term in the k_{sgs} equation are shown. As can be seen they are fairly much in balance. The spatial variation of $\langle C_*\rangle_t$ is also included.

5. Conclusions and Future Work

This is the first contribution towards a development of a new dynamic subgrid model. The general idea is to include dynamic information in the source terms of an equation for the turbulent kinetic subgrid energy k_{sgs} rather than directly in the momentum equations. In the momentum equation a *homogeneous* value (keeping the time dependence) of the local dynamic coefficient is used. In this way numerical stability is greatly enhanced since the large oscillation in the local dynamic coefficients enter as source terms in the k_{sgs} equation, and they are naturally smoothed out through convection and diffusion. This model naturally accounts for back-scatter since the

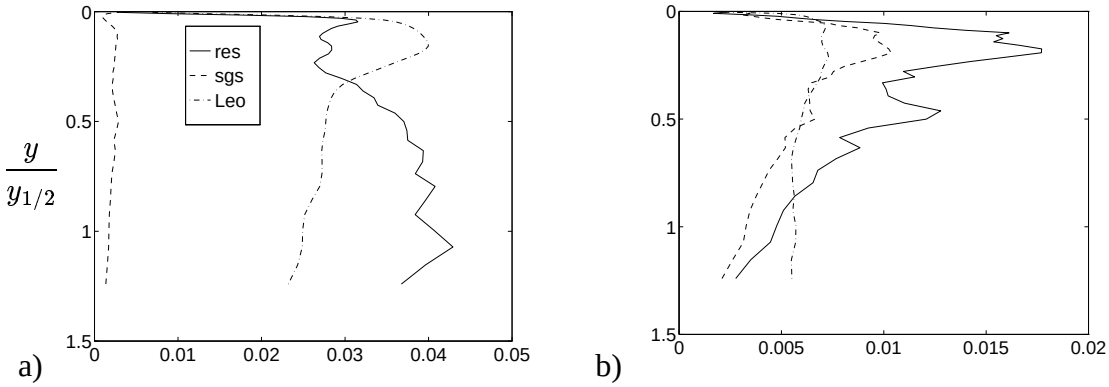

Figure 7: Symmetry plane $z/H = 0.5$. $x/h = 40$. a) Kinetic turbulent energies. Solid line: resolved turbulent kinetic energy $\frac{1}{2}\langle u_i'' u_i'' \rangle_t / U_{in}^2$; dash-dotted line: kinetic energy of dynamic Leonard stresses $\frac{1}{2}\mathcal{L}_{ii}/U_{in}^2$; dashed line: turbulent kinetic subgrid energy $\langle k_{sgs} \rangle_t / U_{in}^2$. b) Terms in the in the subgrid kinetic energy equation. Solid line: production $\langle P_k \rangle_t$; dashed line: dissipation $\langle C_* k_{sgs}^{1.5}/\Delta \rangle_t$; dash-dotted line: $0.001\langle C_* \rangle_t$.

production term in the k_{sgs} equation is permitted to go negative.

It was found that the current form for computing the local dynamic coeffi cient in front of the dissipation term is not a good choice. The reason is that the coeffi cient tends to oscillate between its minimum and maximum permitted values due to a positive feedback. One way to avoid this problem is to, instead of using an ASM-like expression (Eq. 6), assume that the right-hand sides of the k_{sgs} and K equation are equal (see Eq. 5), i.e.

$$\widehat{P}_{k_{sgs}} - \frac{\widehat{C_* k_{sgs}^{\frac{3}{2}}}}{\Delta} = P_K - C_* \frac{K^{\frac{3}{2}}}{\widehat{\Delta}} \quad \Rightarrow \quad C_*^{n+1} = \left(P_K - \widehat{P}_{k_{sgs}} + \frac{1}{\Delta} \widehat{C_*^n k_{sgs}^{\frac{3}{2}}} \right) \frac{\widehat{\Delta}}{K^{\frac{3}{2}}}.$$

References

1. M. Germano, U. Piomelli, P. Moin, and W.H. Cabot. A dynamic subgrid-scale eddy viscosity model. *Phys. Fluids A*, 3:1760–1765, 1991.
2. M. Germano, U. Piomelli, P. Moin, and W.H. Cabot. Erratum. *Phys. Fluids A*, 3:3128, 1991.
3. K.-S. Yang and J.H. Ferziger. Large-eddy simulation of turbulent obstacle fbw using a dynamic subgrid-scale model. *AIAA J.*, 31:1406–1413, 1993.
4. U. Piomelli. High Reynolds number calculations using the dynamic subgrid-scale stress model. *Phys. Fluids A*, 5:1484–1490, 1993.
5. Y. Zang, R.L. Street, and J.R. Koseff. A dynamic mixed subgrid-scale model and its application to turbulent recirculating fbws. *Phys. Fluids A*, 5:3186–3196, 1993.
6. U. Piomelli and L. Junhui. Large-eddy simulation of rotating channel fbw using a localized dynamic model. *Phys. Fluids*, 7:839–848, 1995.
7. B. Balaras, C. Benocci, and U. Piomelli. Finite-difference computations of high Reynolds number fbw using the Dynamic subgrid-scale model. *Theor. and Comp. Fluid Dyn.*, 7:207–216, 1995.
8. P.R. Voke, S. Gao, and D. Leslie. Large-eddy simulations of plane impinging jets. *Int. J. Numer. Meth. Engng.*, 38:489–507, 1995.
9. L. Davidson and P. Nielsen. Large eddy simulations of the fbw in a three-dimensional

ventilated room. In S. Murakami, editor, *5th Int. Conf. on Air Distributions in Rooms, ROOMVENT'96*, volume 2, pages 161–168, Yokohama, Japan, 1996.[1]

10. M. Olsson. *Large Eddy Simulation of Turbulent Jets*. PhD thesis, Dep. of Mechanics, Royal Institute of Technology, Stockholm, 1997.
11. M. Olsson and L. Fuchs. Large eddy simulation of the proximal region of a spatially developing circular jet. *Phys. Fluids A*, 8:2125–2137, 1996.
12. S. Ghosal, T.S. Lund, P. Moin, and K. Akselvoll. A dynamic localization model for large-eddy simulation of turbulent fbws. *Journal of Fluid Mechanics*, 286:229–255, 1995.
13. S. Ghosal, T.S. Lund, P. Moin, and K. Akselvoll. Corrigendum. *Journal of Fluid Mechanics*, 297:402, 1995.
14. K. Akselvoll and P. Moin. Large eddy simulation of turbulent confi ned coannular jets and turbulent fbw over a backward facing step. Report no. TF-63, Stanford University, Dept. Mech. Eng., 1995.
15. L. Davidson. Large eddy simulations: A note on derivation of the equations for the subgrid turbulent kinetic energies. Rept. 97/11, Dept. of Thermo and Fluid Dynamics, Chalmers University of Technology, Gothenburg, 1997.[1]
16. M. Germano. Turbulence: the fi ltering approach. *Journal of Fluid Mechanics*, 238:325–336, 1992.
17. W. Rodi. A new algebraic relation for calculating the Reynolds stresses. *ZAMM*, 56:T219–T221, 1976.
18. Rodi W. *Turbulence Models and Their Application in hydraulics - a State of the Art Review*. International Association of Hydraulic Research, Monograph, Delft, 1984.
19. H. Nilsson. A parallel multiblock extension to the CALC-BFC code using PVM. Rept. 97/11, Dept. of Thermo and Fluid Dynamics, Chalmers University of Technology, Gothenburg, 1997.[1]
20. P. Emvin and L. Davidson. Development and implementation of a fast large eddy simulations method. *submitted for journal publication*, 1997.
21. C.M. Rhie and W.L. Chow. Numerical study of the turbulent fbw past an airfoil with trailing edge separation. *AIAA J.*, 21:1525–1532, 1983.
22. L. Davidson. Implementation of a large eddy simulation method applied to recirculating fbw in a ventilated room. Report, ISSN 1395-7953 R9611, Dep. of Building Technology and Structural Engineering, Aalborg University, 1996.[1]
23. A. Restivo. *Turbulent Flow in Ventilated Rooms*. PhD thesis, University of London, Imperial College of Science and Technology, Mechanical Engineering Department, 1979.
24. P.V. Nielsen. Specifi cation of a two-dimensional test case. Report, ISSN 0902-7513 R9040, Dept. of Building Technology and Structural Engineering, Aalborg Universitetscenter, Aalborg, 1990.
25. R.I. Karlsson, J. Eriksson, and J. Persson. LDV measurements in an plane wall jet in a large enclosure. In D.F.G Durõ R.J. Adrian, F. Durst, M. Heitor, M. Maeda, and J. H J.H. Whitelaw, editors, *Laser Techniques and Applications in Fluid Mechanics*, pages 311–332. Springer-Verlag, 1993.

[1] available as postscript fi le at http://www.tfd.chalmers.se/~lada